Biochimica et Biophysica Acta 1837 (2014) 1922–1931

Contents lists available at ScienceDirect

Biochimica et Biophysica Acta

journal homepage: www.elsevier.com/locate/bbabio

The D1-173 amino acid is a structural determinant of the critical interaction between D1-Tyr161 (Tyr_Z) and D1-His190 in Photosystem II

Miwa Sugiura [a,b,c,*], Yui Ozaki [a], Masato Nakamura [b], Nicholas Cox [d], Fabrice Rappaport [e], Alain Boussac [f,**]

[a] Proteo-Science Research Center, Ehime University, Bunkyo-cho, Matsuyama Ehime, 790-8577, Japan
[b] Department of Chemistry, Graduate School of Science and Technology, Ehime University, Bunkyo-cho, Matsuyama, Ehime 790-8577, Japan
[c] PRESTO, Science and Technology Agency (JST), 4-1-8, Honcho, Kawaguchi, Saitama 332-0012, Japan
[d] Max-Planck-Institut für Chemische Energiekonversion, Stiftstrasse 34-36, D-45470 Mülheim an der Ruhr, Germany
[e] Institut de Biologie Physico-Chimique, UMR 7141 CNRS and Université Pierre et Marie Curie, 13 rue Pierre et Marie Curie, 75005 Paris, France
[f] iBiTec-S, CNRS UMR 8221, CEA Saclay, 91191 Gif-sur-Yvette, France

ARTICLE INFO

Article history:
Received 8 July 2014
Received in revised form 20 August 2014
Accepted 26 August 2014
Available online 2 September 2014

Keywords:
Photosystem II
PsbA
D1
Thermosynechococcus elongatus
Tyr_Z
Proline

ABSTRACT

The main cofactors of Photosystem II (PSII) are borne by the D1 and D2 subunits. In the thermophilic cyanobacterium *Thermosynechococcus elongatus*, three *psbA* genes encoding D1 are found in the genome. Among the 344 residues constituting the mature form of D1, there are 21 substitutions between PsbA1 and PsbA3, 31 between PsbA1 and PsbA2, and 27 between PsbA2 and PsbA3. In a previous study (Sugiura et al., J. Biol. Chem. 287 (2012), 13336-13347) we found that the oxidation kinetics and spectroscopic properties of Tyr_Z were altered in PsbA2-PSII when compared to PsbA(1/3)-PSII. The comparison of the different amino acid sequences identified the residues Cys144 and Pro173 found in PsbA1 and PsbA3, as being substituted in PsbA2 by Pro144 and Met173, and thus possible candidates accounting for the changes in the geometry and/or the environment of the Tyr_Z/His190 phenol/imidizol motif. Indeed, these amino acids are located upstream of the α-helix bearing Tyr_Z and between the two α-helices bearing Tyr_Z and its hydrogen-bonded partner, D1/His190. Here, site-directed mutants of PSII, PsbA3/Pro173Met and PsbA2/Met173Pro, were analyzed using X- and W-band EPR and UV-visible time-resolved absorption spectroscopy. The Pro173Met substitution in PsbA2-PSII *versus* PsbA3-PSII is shown to be the main structural determinant of the previously described functional differences between PsbA2-PSII and PsbA3-PSII. In PsbA2-PSII and PsbA3/Pro173Met-PSII, we found that the oxidation of Tyr_Z by $P_{680}^{+\bullet}$ was specifically slowed during the transition between S-states associated with proton release. We thus propose that the increase of the electrostatic charge of the Mn_4CaO_5 cluster in the S_2 and S_3 states could weaken the strength of the H-bond interaction between $Tyr_Z^{\bullet}$ and D1/His190 in PsbA2 *versus* PsbA3 and/or induce structural modification(s) of the water molecules network around Tyr_Z.

1. Introduction

The light-driven oxidation of water in Photosystem II (PSII) is the first step in the photosynthetic production of most of the earth's-biomass, fossil fuels and O_2. The PSII super-complex in cyanobacteria is made up of 17 membrane protein subunits and 3 extrinsic proteins, capping the site of water splitting catalysis (PsbY was not present in [1] but observed in [2]). The homologous membrane proteins D1 and D2 form the center of the super-complex. They bind all key cofactors/redox centers involved in primary charge separation, electron transfer and water splitting/plastoquinone reduction catalysis [1]. The excitation resulting from the absorption of a photon is transferred to the photochemical trap (reaction center) that undergoes charge separation. The reaction center consists of four chlorophyll *a* molecules, P_{D1}/P_{D2} and Chl_{D1}/Chl_{D2}, and two pheophytin *a* molecules, Phe_{D1}/Phe_{D2}. The resulting positive charge is then stabilized on P_{680} (an excited state of mainly P_{D1}/P_{D2} character). $P_{680}^{+\bullet}$ then oxidizes a nearby redox active tyrosine, Tyr_Z, the Tyr161 of the D1 polypeptide, which in turn oxidizes an inorganic Mn_4CaO_5 cluster. On the electron acceptor side the electron is transferred to the primary quinone electron acceptor, Q_A, and then to Q_B, a two-electron and two-proton acceptor, *e.g.* [3–5]. The Mn_4CaO_5 cluster accumulates

Abbreviations: PSII, Photosystem II; Chl, chlorophyll; MES, 2-(N-morpholino) ethanesulfonic acid; P_{680}, chlorophyll dimer acting as the electron donor; Q_A, primary quinone acceptor; Q_B, secondary quinone acceptor; Cm, chrloramphenicol; Sm, streptmycin; Sp, spectinomycin; 43H, *T. elongatus* strain with a His-tag on the C terminus of CP43; PQ, plastoquinone 9; WT*1, WT*2, WT*3, cells containing only the $psbA_1$, $psbA_2$, $psbA_3$ gene, respectively; $Pheo_{D1}$, pheophytin; P_{D1} and P_{D2}, Chl monomer of P_{680} on the D1 or D2 side, respectively; PPBQ, phenyl *p*-benzoquinone; β-DM, *n*-dodecyl-β-maltoside; NIR, near-infrared; CW, continuous wave; MALDI-TOF, matrix-assisted laser desorption/ionization-time of flight

* Correspondence to: M. Sugiura, Proteo-Science Research Center, Ehime University, Bunkyo-cho, Matsuyama Ehime, 790-8577, Japan.
** Corresponding author.
E-mail addresses: miwa.sugiura@ehime-u.ac.jp (M. Sugiura), alain.boussac@cea.fr (A. Boussac).

http://dx.doi.org/10.1016/j.bbabio.2014.08.008
0005-2728/

oxidizing equivalents and acts as the catalytic site for water oxidation. The enzyme cycles sequentially through five redox states denoted S_n where n stands for the number of stored oxidizing equivalents. Upon formation of the S_4 state two molecules of water are rapidly oxidized, O_2 is released and the S_0 state is regenerated [4–9].

Cyanobacterial species have multiple *psbA* variants encoding for the D1 protein, *e.g.* [10–22]. These gene homologues are known to be differentially transcribed depending on the environmental conditions, see [23] for a recent discussion. The genome of the thermophilic cyanobacterium *Thermosynechococcus elongatus* contains three different *psbA* genes [24]. Among the 344 residues of the matured PsbA proteins, 21 differ between PsbA1 and PsbA3, 31 between PsbA1 and PsbA2 and 27 between PsbA2 and PsbA3. The $psbA_1$ gene is constitutively expressed under "general" laboratory conditions, while the $psbA_3$ gene is transcribed under light stress conditions such as high light or UV light conditions [14,25,26]. The transcription of the $psbA_2$ gene has been reported to increase under micro-aerobic conditions [16]. Notably, D1 transcription/regulation may vary among cyanobacteria. In *T. elongatus*, the differential transcription patterns of the three genes coding for the D1 subunit raise the possibility that, in this species, the regulation at the transcription level represents an acclimation mechanism where the functional properties of PSII are adjusted to cope with the increased photon flux, *e.g.* the interchange of the PsbA1 and PsbA3 variants modifies the redox potential of $Pheo_{D1}$ [23]. Changes in the already identified properties of the redox cofactors depending on the D1 variant constituting PSII in *T. elongatus* have been recently reviewed [27].

The effects of the PsbA(1/3)/PsbA2 substitution are much less documented. In a previous study [28], we showed, based on the analysis of the kinetic and spectroscopic properties of $Tyr_Z/Tyr_Z^{\bullet}$ and $P_{680}/P_{680}^{+\bullet}$ that the protein structure in the vicinity of the Tyr_Z, likely the hydrogen bond between the phenol group of Tyr_Z and D1/His190, is modified in PsbA2-PSII as compared to PsbA(1/3)-PSII. This change is critical to the function of Tyr_Z as its rapid reversible oxidation by $P_{680}^{+\bullet}$ relies on the shuttling of its phenolic proton to the nitrogen (2.46 Å between the O and N) of D1/His190 forming the stabilized neutral tyrosyl radical [29]. An increase in the distance between the acid/base residues is expected to alter the dynamics of the proton coupled electron transfer processes associated with the oxidation of Tyr_Z [30]. Proline is known to constrain the specific angles of the NH-C=O peptide bond and thus to possibly change the orientation of the downstream helix, *e.g.* [31]. Thus we hypothesized that the Cys144 to Pro144 and Pro173 to Met173 substitutions in PsbA2 from PsbA1 and PsbA3, located upstream of the α-helix bearing Tyr_Z and between the two α-helices bearing Tyr_Z (helix C in Fig. 1) and its hydrogen-bonded partner, D1/His190 (helix D in Fig. 1) were responsible for the differences in the structure of the Tyr_Z-His190 couple (Fig. 1). PsbA2 in *T. elongatus* represents one of the few photosynthetic species already sequenced in which the D1-173 amino acid is not a Pro. These include PsbA0 in *Anabaena* (*alr3742*) with a Met and D1-4 in *Gloeobacter violaceus* PCC 7421 (*glr1706*) with a Ser. Therefore, in order to assess the hypothesis according to which substituting Met173 for Pro173 in PsbA2 for PsbA3 accounts for the structural changes in the vicinity of Tyr_Z and thus for the functional characteristics described above, we used these two observables and compared the sets of pairs: the PsbA3/Pro173Met and PsbA2/Met173Pro pair and the PsbA2-PSII and PsbA3-PSII pair.

In this work, using EPR spectroscopy and time resolved absorption spectroscopy, site directed-mutants of the amino acid residue at position 173 in PsbA2 and PsbA3 were studied by reengineering PsbA2 to mimic the PsbA3 structure for Tyr_Z and *vice versa*. In the PsbA3/Pro173Met-PSII and PsbA2/Met173Pro-PSII mutants, we show that the Pro173Met substitution in PsbA2-PSII *versus* PsbA3-PSII is the main structural parameters that affects the electron transfer between Tyr_Z and P_{680}.

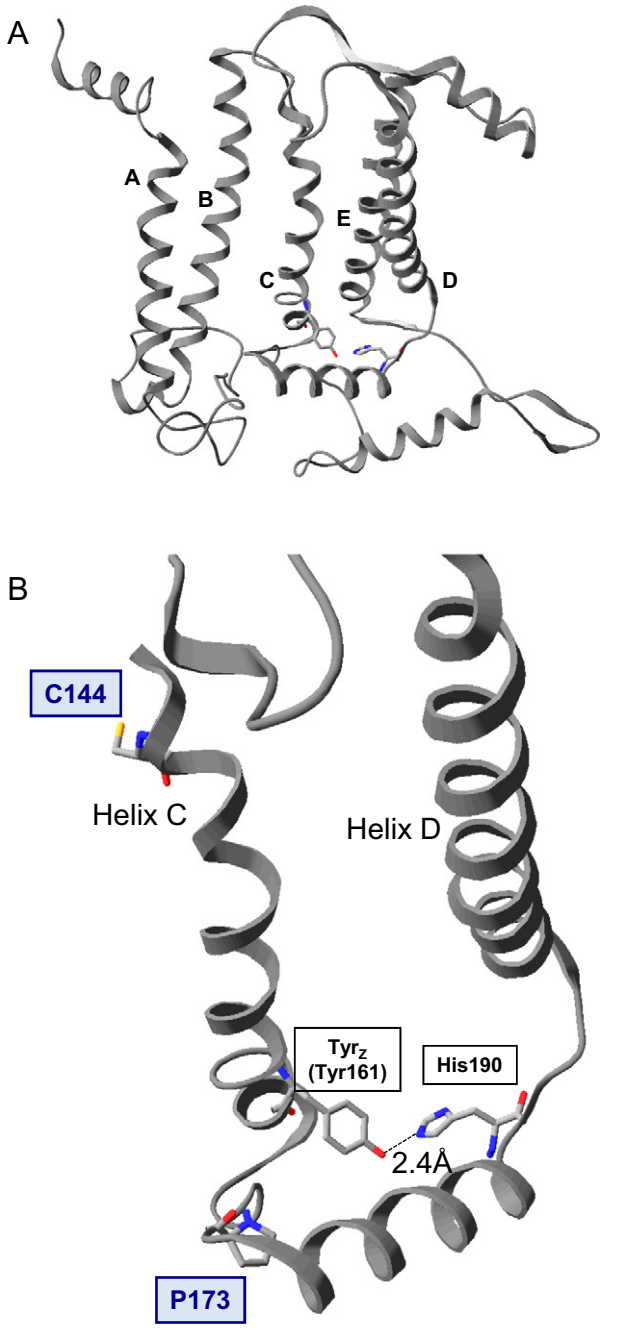

Fig. 1. Structure of D1 helices (A) and around Tyr_Z and His190 (B) from the 1.9 Å resolution structure model of Umena et al. [1]. Tyr_Z (D1/Tyr161) and His190 are belonging to helix C and helix D, respectively. The H-bond distance between Tyr_Z and His190 is 2.4 Å. Pro173 and Cys144 in PsbA2 and PsbA3 were substituted. Figures were drawn with Swiss Pdb Viewer with PDB 3ARC.

2. Materials and methods

2.1. T. elongatus mutant strains

In this study, purified PSII from *T. elongatus* WT*2 [28] and WT*3 [32] cell strains were used as controls. WT*2 and WT*3 are both His-tagged strains on the C-terminus of CP43 [33] with PsbA2 and PsbA3 as the D1 protein by deletion of $psbA_1/psbA_3$ and $psbA_1/psbA_2$, respectively [28,32]. Fig. 2A shows a map of the constructed plasmid DNA, pUPsbA2/Cm for making the PsbA2/Met173Pro site directed mutant in *T. elongatus*. For the expression of the $psbA_2$ gene under the control of the $psbA_3$ promoter instead of the $psbA_2$ promoter, a 1291 bp DNA

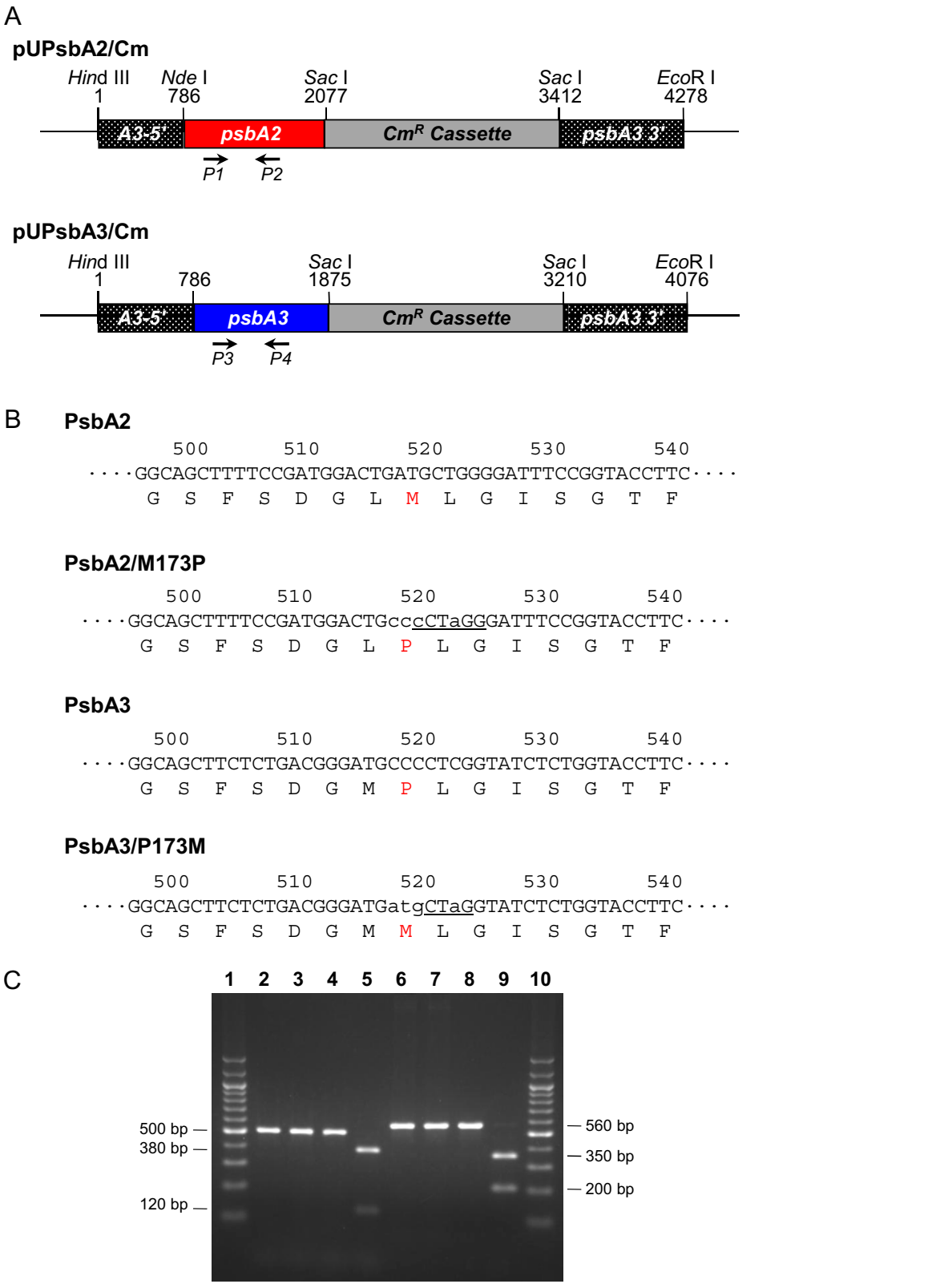

Fig. 2. (A) Map around site-directed *psbA*$_2$ *and psbA*$_3$ of *T. elongatus* mutant genome. The open reading frame of *psbA*$_2$ gene was ligated downstream of the *psbA*$_3$ promoter to express *psbA*$_2$ under the control of the *psbA*$_3$ promoter. A chloramphenicol (Cm) resistant cassette was inserted between the *psbA*$_2$ gene and downstream of *psbA*$_3$ at *Sac* I sites. For expression of PsbA3, a Cm resistant cassette was inserted after *psbA*$_3$ gene. (B) The nucleotides and translated amino acids sequences of PsbA2, PsbA2/Met173Pro, PsbA3, and PsbA3/Pro173Met wild type including amino acid position of 173. Newly created restriction enzyme sites for site-directed mutations are underlined. *Avr* II and *Bfa* I sites were newly created for PsbA2/Met173Pro and PsbA3/Pro173Met mutants, respectively. (C) Agarose gel (1%) electrophoresis of amplified products by PCR using *P1* and *P2* primers indicated in Fig. 2A (lanes 2–5), and digested the amplified DNA fragments with *Avr* II (lanes 3 and 5). Amplified PCR products using *P3* and *P4* primers are indicated in Fig. 2A (lanes 6–9), and digested the amplified DNA fragments with *Bfa* I (lanes 7 and 9). Lanes 1 and 10, 1 kb DNA ladder markers (Nakarai Co., Japan Lane 13 and 14); lanes 2 and 3, WT*2; lanes 3 and 4, PsbA2/Met173Pro mutant; lanes 6 and 7, WT*3; lanes 8 and 9, PsbA3/Pro173Met mutant.

fragment containing the open reading frame was inserted into created *Nde* I site on $psbA_3$ promoter region and *Sac* I site. This *Nde* I site was created by a Site-directed Mutagenesis Lightning Kit (Stratagene) at the same position of the initial codon of $psbA_3$. Next, non-coding 3′-region (≈800 bp) of $psbA_3$ was ligated at *Sac* I and *Eco*R I sites. Then, chloramphenicol resistant (Cm^R) cassette was inserted downstream of stop codon of $psbA_2$ and 3′-region of $psbA_3$ at Sac 1 sites. For creation of site-directed mutations on PsbA2, the nucleotides were modified containing new restriction enzyme site, *Avr* II, using a Site-directed Mutagenesis Lightning Kit (Stratagene) as shown in Fig. 2B. Fig. 2A shows a map of the constructed plasmid DNA, pUPsbA2/Cm for making the PsbA2/Met173Pro site directed mutant. In this case, the $psbA_3$ gene expression was controlled by naturally $psbA_3$ promoter. A Cm^R cassette was inserted as well as pUPsbA2/Cm. The nucleotides were modified in order to insert a new restriction enzyme site, *Bfa* I, using a Site-directed Mutagenesis Lightning Kit (Stratagene) as shown in Fig. 2B.

The constructed plasmid pUPsbA2/Met173Pro and pUPsbA3/Pro173Met were introduced into WT*3 cells by electroporation (Gene Pulser Xcell, Bio-Rad) as following [28,32,33]. The *T. elongatus* transformants were selected as single colonies on DTN agar plate [33] containing appropriate antibiotics (25 μg mL^{-1} of spectinomycin, 10 μg mL^{-1} of streptomycin, 40 μg mL^{-1} of kanamycin and 5 μg mL^{-1} of chloramphenicol). Segregation of all genome copies was confirmed by digestion of amplified DNA fragments including the site-directed mutations by PCR with restriction enzyme. For PsbA2/Met173Pro selection, 500 bp of DNA amplified fragments by *P1* primer (5′-GCTACCGTCT CGGTATGCGGCCTTGGATTC-3′) and *P2* primer (5′-GAAACCATTGAGGT TAAAGGCCATCGTGCT-3′) was digested with *Avr* II to separate 380 bp and 120 bp (results showed in Fig. 2C, lanes 2–5). For selection and confirmation of PsbA3/Pro173Met, amplified 560 bp of DNA fragments by *P3* primer (5′-CTACAACGGTGGCCCCTACCAACTG-3′) and *P4* primer (5′-GCTGATACCCAGGGCAGTAAACCAGATGCC-3′) were digested with *Bfa* I to give 350 bp and 210 bp (results showed in Fig. 2C, lanes 6–9).

2.2. Cultivation of mutant cells and purification of PSII core complexes

Cells were grown in 1 L of DTN in 3-L Erlenmeyer flasks in a rotary shaker with a CO_2-enriched atmosphere at 45 °C under continuous light (≈80 μmol of photons m^{-2} s^{-1}) until they reached an optical density (O.D.) close to 1.0 at 800 nm. After harvesting by centrifugation, the cells were washed once with buffer 1 (1 M betaine, 10 % glycerol, 40 mM MES, 15 mM $MgCl_2$, 15 mM $CaCl_2$, pH 6.5 (adjusted with NaOH)) and resuspended in the same buffer, with 0.2% (w/v) bovine serum albumin, 1 mM benzamidine, 1 mM ε-aminocaproic acid, and ≈50 μg mL^{-1} DNase I added, to a chlorophyll concentration of ≈1.5 mg Chl mL^{-1}. The cells were ruptured with a French press. Unbroken cells were removed by centrifugation (3000×*g*, 5 min). Membranes were pelleted by centrifugation at 180,000 *g* for 30 min at 4 °C and washed twice with buffer 1. Thylakoids (1 mg Chl mL^{-1}, final concentration after the addition of the detergent) were treated with 0.8 % (w/v) n-dodecyl-β-maltoside (β-DM, Biomol, Germany) in buffer 1 supplemented with 100 mM NaCl. After ≈1 min of stirring in the dark at 4 °C the suspension was centrifuged (20 min, 170,000 *g*) to remove the non-solubilized material. Then, the supernatant was mixed with an equal volume of ProBond resin (Invitrogen, Groningen, The Netherlands) that had been pre-equilibrated with buffer 1. The resulting slurry was transferred to an empty column. After sedimentation of the resin inside the column, the supernatant was removed. The resin was washed with buffer 2 (1 M betaine, 10 % glycerol, 40 mM MES, 15 mM $MgCl_2$, 15 mM $CaCl_2$, 100 mM NaCl, 1 mM L-histidine, 0.03% (w/v) β-DM, pH 6.5) until the OD value of the eluate at ≈665 nm decreased below 0.05 (approximately 15 hours). Then, PSII core complexes were eluted with buffer 3 (1 M betaine, 40 mM MES, 15 mM $MgCl_2$, 15 mM $CaCl_2$, 200 mM NaCl, 180 mM L-histidine, 0.06% (w/v) β-DM, pH 6.5). The eluate was then concentrated and washed in buffer 4 with 1 M betaine, 40 mM MES, 15 mM $MgCl_2$, 15 mM $CaCl_2$, pH 6.5, using centrifugal filter devices (Ultrafree-15, Millipore). PSII core complexes were finally resuspended in the same buffer at a Chl concentration of ≈1.5-2.0 mg Chl mL^{-1} and stored in liquid N_2 before to be used.

2.3. Mn-depletion

For the Mn-depletion of the samples, the PSII were diluted approximately 10-fold in a medium containing 1.2 M Tris-HCl (pH 9.2) and were incubated under room light at 4 °C for 1 h. The samples were then collected by centrifugation for 3 h at 600,000×*g*. Then the pellet was resuspended in buffer 4. After a second centrifugation for 3 h at 600000 g the pellet was resuspended in buffer 4 at ≈1.5–2.0 mg Chl mL^{-1} and stored in liquid N_2 before to be used.

2.4. P_{680}^{+} reduction kinetics measurements

Time resolved absorption changes were measured with a lab-built spectrophotometer [34] where the absorption changes are sampled at discrete times by short flashes. These flashes were provided by a neodymium:yttrium-aluminum garnet (Nd:YAG, 355 nm) pumped optical parametric oscillator, which produces monochromatic flashes (1 nm full-width at half-maximum) with a duration of 5 ns. Excitation was provided by a second neodymium:yttrium–aluminum garnet (Nd:YAG, 532 nm) pumped optical parametric oscillator, which produces monochromatic saturating flashes at 700 nm (1 nm full-width at half-maximum) with a duration of 5 ns. The path length of the cuvette was 2.5 mm. PSII was used at 25 μg of Chl mL^{-1} in 1 M betaine, 15 mM $CaCl_2$, 15 mM $MgCl_2$, and 40 mM MES (pH 6.5). PSII were dark-adapted for ≈1 h at room temperature (20–22 °C) before the addition of either 0.1 mM phenyl p-benzoquinone (PPBQ) dissolved in dimethyl sulfoxide. For kinetic measurements, the time delay between the actinic flash and the detector flash was first increased from the smaller value to the larger value and then varied in the opposite direction. For each time delay the measurements were repeated 4 times so that each data point is the average of 8 measurements.

2.5. EPR measurements

X-band cw-EPR spectra were recorded with a Bruker Elexsys 500 X-band spectrometer equipped with a standard ER 4102 (Bruker) X-band resonator, a Bruker teslameter, an Oxford Instruments cryostat (ESR 900) and an Oxford ITC504 temperature controller. Flash illumination at room temperature was provided by a Nd:YAG laser (532 nm, 550 mJ, 8 ns Spectra Physics GCR-230-10). PSII samples at 1.1 mg of Chl mL^{-1} were loaded in the dark into quartz EPR tubes and dark-adapted for 1 h at room temperature. Then, the samples were synchronized in the S_1-state with one pre-flash [35]. After a further 1 h dark-adaptation at room temperature the samples were illuminated by two additional flashes to generate the S_3 state before to be frozen in the dark to 198 K and then transferred to 77 K. In both cases the samples were degassed at 198 K prior to the recording of the spectra. Near-IR illumination of the samples was done directly in the EPR cavity, at 4.2 K, and was provided by a laser diode emitting at 820 nm (Coherent, diode S-81-1000C) with a power of 600–700 mW at the level of the sample.

W-band (~94 GHz) EPR experiments were performed at 15 K using a Bruker ELEXSYS E680 EPR spectrometer. Two-pulse electron spin echo (ESE)-detected field-swept EPR spectra were measured using the pulse sequence $t_p - \tau - 2t_p - \tau -$ echo. The length of the π microwave pulses was set to 56 ns and inter-pulse distances were 300 ns. The echo was integrated ~600 ns around its maximum. The shot repetition time was 3 ms.

2.6. Measurements of O_2 evolution activity

Oxygen evolution activity of purified PSII (5 μg Chl mL^{-1}) was measured under continuous saturating white light at 25 °C by polarography

using a Clark type oxygen electrode (Hansatech). A total of 0.5 mM 2,6-dichloro-*p*-benzoquinone (dissolved in dimethyl sulfoxide) was added as an electron acceptor.

3. Results

3.1. Expression of site-directed PsbA2/Met173Pro and PsbA3/Pro173Met mutants in T. elongatus

In our previous study [28] comparing the PsbA2-PSII and PsbA3-PSII homologues, two important differences were observed; i) the rate of reduction of $P_{680}^{+\bullet}$ by Tyr_Z in PsbA2-PSII was slower than that in PsbA3-PSII in the S_2 and S_3 states, but, importantly, remained unchanged in the S_1 state, and ii) the magnetic properties of the Tyr_Z were modified. These latter properties were assessed using time resolved absorption changes and EPR spectroscopies. In wild type of *T. elongatus*, the $psbA_2$ gene is not transcribed efficiently [25,26]. However, although the transcription of $psbA_3$ in WT is induced by light stresses such as high light or UV light [14,25,26], we have shown that WT*3 cells (*i.e.* the $\Delta psbA_1/\Delta psbA_2$ deletion mutant) efficiently express PsbA3 as D1 under the control of the $psbA_3$ promoter, reviewed in [27]. Therefore, in this study, the construction of the PsbA2/Met173Pro mutant was done so that the expression of D1 was also under the control of the $psbA_3$ promoter as shown in Fig. 2A.

The comparison of the polypeptide content of purified PsbA2/Met173Pro and PsbA3/Pro173Met with that of PsbA2-PSII and PsbA3-PSII was achieved by SDS-polyacrylamide gel electrophoresis and MALDI-TOF/mass spectroscopy (data not shown). PSII complexes isolated from both mutants, PsbA3-PSII and PsbA2-PSII complexes were composed of 20 subunit proteins. Notably, the migration of the D1 protein was found slightly faster in PsbA2-PSII (38199 Da, lane 3) than in PsbA3-PSII (38259 Da, lane 1) as observed previously [36] (Fig. 3). However, the migration of the D1 protein was found similar in PsbA3-PSII and PsbA3/Pro173Met-PSII (38213 Da, lane 2) and in PsbA2-PSII and PsbA2/Met173Pro-PSII (38165 Da, lane 4). So, the reason of the D1 migration modifications in PsbA2-PSII is not the Pro173Met exchange alone and remains an open question to be addressed in future studies.

3.2. Effects of the mutations on the water splitting activity

It has been reported earlier that the oxygen evolution activity of PsbA2-PSII was slightly lower than that of PsbA3-PSII [28]. This was proposed to originate from changes at the electron acceptor side because the kinetics of the $S_3Tyr_Z^{\bullet}$ to S_0Tyr_Z transition were found similar in PsbA2-PSII and PsbA3-PSII. The O_2 evolution activity of purified PsbA3/Pro173Met PSII and PsbA2/Met173Pro-PSII was ≈2000 μmol O_2 $(mg\ Chl)^{-1}\ h^{-1}$. So, the activity of PsbA3/Pro173Met-PSII was decreased when compared to PsbA3-PSII (≈3500 μmol O_2 $(mg\ Chl)^{-1}\ h^{-1}$) whereas the activity of PsbA2/Met173Pro was almost the same as that of PsbA2-PSII. It should be noted, however, that the oxygen evolution activity of whole cells was similar in the four strains, *i.e.* about 180–220 μmol O_2 $(mg\ Chl)^{-1}\ h^{-1}$.

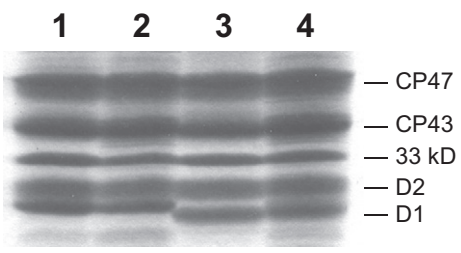

Fig. 3. SDS-polyacrylamide gel electrophoresis of isolated PSII complexes range of about 50 to 30 kDa. Lane 1, PsbA3-PSII; lane 2, PsbA3/Pro173Met-PSII; lane 3, PsbA2-PSII and lane 4, PsbA2/Met173Pro-PSII. The amount of PSII loaded was 10 μg of Chl for each lane.

3.3. Low temperature EPR spectroscopy: Substitution of D1-Pro173 to Met modifies the magnetic interaction between Tyr_Z and the Mn_4CaO_5 cluster

To be detectable by EPR spectroscopy, Tyr_Z must be in its oxidized (radical) form. Under physiological conditions, the oxidized Tyr_Z is generated via oxidation by $P_{680}^{+\bullet}$. The oxidized Tyr_Z is then rapidly reduced by the Mn_4CaO_5 cluster, preventing its characterization by EPR owing to the inappropriate time resolution of the method. A long-lived oxidized Tyr_Z can however be generated by near-infrared photo-excitation of the Mn_4CaO_5 cluster at cryogenic temperatures (≈4.2 K). This induces an electron transfer reaction involving Tyr_Z, which is oxidized, and the Mn_4CaO_5 cluster, which is reduced [37]. The yield of Tyr_Z oxidation is dependent on the S-state in which it is poised with NIR illumination of the Mn_4CaO_5 in the S_3 state giving the highest yield [37,38]. Thus, it is this state, $(S_2Tyr_Z^{\bullet})'$, in which we have investigated the oxidized tyrosine. As the $Tyr_Z^{\bullet}$ radical is in close proximity to the Mn_4CaO_5 cluster, it displays a perturbed EPR signal described in the literature as a split signal. The precise structure of the split signal is sensitive to the spin state of the Mn_4CaO_5 cluster and is thus S-state dependent. The split signal associated with the $(S_2Tyr_Z^{\bullet})'$ state is attributed to the magnetic interaction between $Tyr_Z^{\bullet}$, a spin $S = 1/2$ center, and the Mn_4CaO_5 cluster in an $S \geq 5/2$ spin configuration [39]. It is thus expected to be sensitive to the Pro to Met substitution if indeed Pro constrains the NH-C = O peptide bond and thus bends the orientation of the downstream helix, thereby affecting the structure in the vicinity of Tyr_Z.

Fig. 4 shows the EPR difference spectra after-*minus*-before near-infrared illumination of the enzyme poised in the S_3 state in PsbA3-PSII (black), in PsbA2-PSII (red), in PsbA3/Pro173Met-PSII (blue) and in PsbA2/Met173Pro-PSII (green). Panel A shows the full EPR spectrum including the magnetic field region where a signal attributed to the Mn_4CaO_5 cluster in the S_2' state peaks at ≈1280 gauss (which corresponds to g ≈5.3) and Panel B shows the split signal region. As described earlier [28], there are manifest differences between PsbA3-PSII and PsbA2-PSII split signals. These differences though are cancelled, or at least diminished, by the mutation of D1/Met173 to Pro in PsbA2, which shows strong similarities with PsbA3-PSII, and in the reciprocal case of the Pro173Met mutation which now resembles the PsbA2-PSII. Importantly these statements not only apply to the spectroscopic features but also to the overall formation yield of the split signal. Both the yield and spectral shape of the split signal are quite similar in PsbA2-PSII and PsbA3/Pro173Met-PSII. Despite remaining differences between the PsbA3-PSII and PsbA2/Met173Pro-PSII, altogether these data show that among the 27 amino acid substitutions between PsbA2-PSII and PsbA3-PSII the Pro173Met exchange is the key structural determinant responsible for changes in the NIR-induced split signal. Panel A in Fig. 4 shows that the spectral shape of the signal originating from the $Mn_4Ca_4O_5$ cluster is very similar in the 4 different PSII samples and therefore likely resilient to the mutations.

3.4. High field (W-band) EPR spectroscopy: The Pro173Met exchange modifies the local site properties of Tyr_Z residue

High field EPR spectroscopy presents a series of advantages for the study of organic radicals such as Tyr. At higher magnetic fields, the local environment of the radical can be assessed as the *g*-matrix can be resolved. The three *g*-matrix values, the turning points in the EPR spectrum, essentially describe the electronic structure of the radical along its three unique axes: i) the axis bisecting the phenolic oxygen/ring plane (g_x); ii) the axis bisecting the ring plane, perpendicular to the phenolic oxygen (g_y); and iii) the axis perpendicular to the ring plane (g_z). The data presented here represent low temperature (15 K) measurements on Tyr_Z radical generated by short illumination (5 s) in the presence of 5 mM ferricyanide, which serves to reoxidize the acceptor side ($Q_A^{-\bullet}$ or $Q_B^{-\bullet}$) of PSII. Importantly, these measurements were performed in PSII samples where the Mn_4CaO_5 cluster was removed by Tris-washing. This allows the EPR spectrum of the uncoupled radical

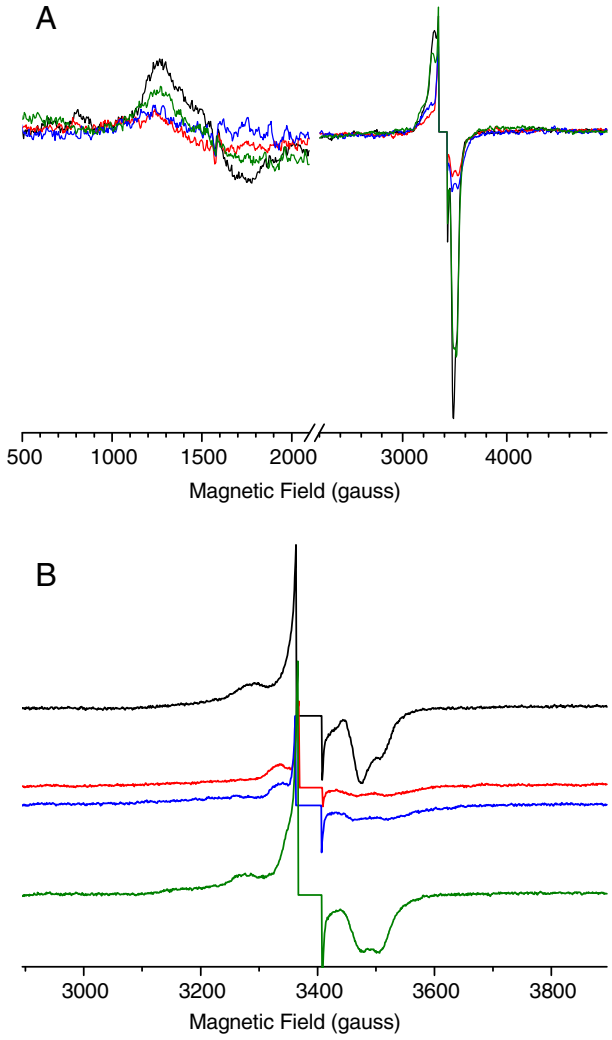

Fig. 4. Near infrared-induced split EPR spectra in PsbA3-PSII (black spectrum), in PsbA2-PSII (red spectrum), in PsbA3-Pro173Met-PSII (blue spectrum) and in PsbA2-Met173Pro-PSII (green spectrum). For the four samples, a spectrum was first recorded after two flashes given at room temperature, and a second spectrum was recorded after a further NIR illumination given in the EPR cavity at 4.2 K. Instrument settings were: modulation amplitude, 25 G; microwave power, 20 mW; microwave frequency, 9.5 GHz; modulation frequency, 100 kHz; and temperature, 4.2 K. The chlorophyll concentration was 1.1 mg.mL^{-1}. The center part corresponding to the $Tyr_D^{\bullet}$ spectrum was deleted. The Panel A shows the full spectrum with a vertical scale magnified fourfold for the low field region and Panel B shows the magnetic field region corresponding to the split signal only.

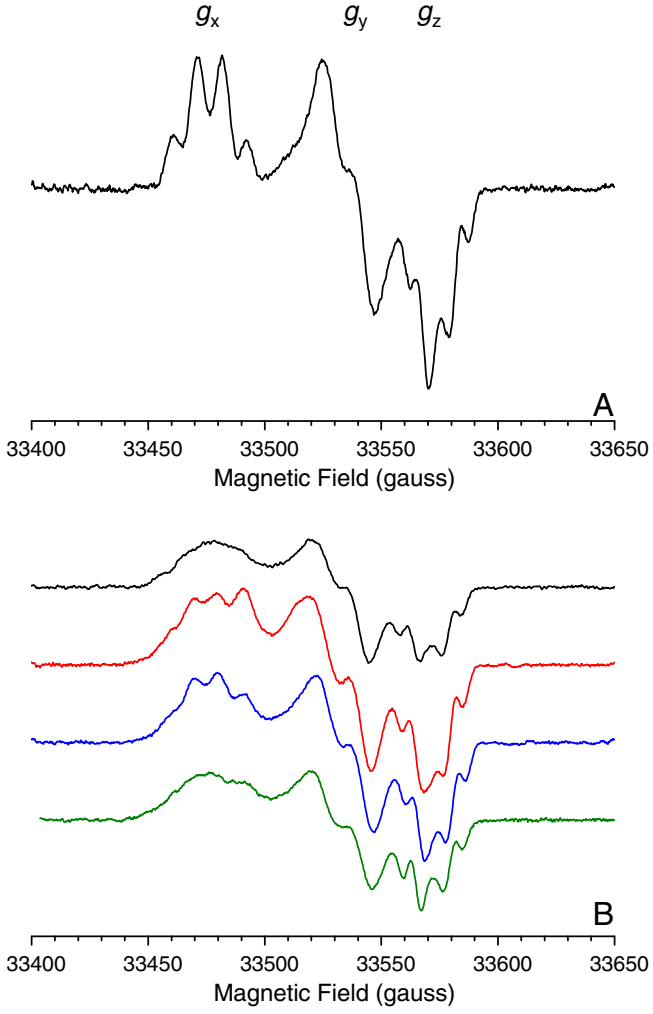

Fig. 5. W-band EPR spectra of $Tyr_D^{\bullet}$ (Panel A) and $Tyr_Z^{\bullet}$ (Panel B) in Mn-depleted PsbA3-PSII (black), PsbA2-PSII (red), PsbA3-Pro173Met-PSII (blue) and PsbA2-Met173Pro-PSII (green). See the Materials and Methods section for further details.

spectrum to be trapped [40] and then measured, which is otherwise broadened by its magnetic interaction with the Mn_4CaO_5 cluster as shown in Fig. 4. We note that an uncoupled Tyr_Z spectrum can also be measured in intact PSII samples at room temperature using time-resolved measurements *e.g.* [28,41] where the fast relaxation of the Mn_4CaO_5 as compared to Tyr_Z can be exploited. While these measurements can be straightforwardly implemented at W-band, they require special setups which would allow the illumination of the samples inside the resonator and the recording of the signal with a sufficient signal-to-noise ratio taking into account the extremely small size of the samples required for such a measurements. The detection of the magnetically uncoupled $Tyr_Z^{\bullet}$ state in intact PSII at frequencies greater than 90 GHz forms ongoing work of our laboratories, see though [42,43].

Panel A in Fig. 5 shows the pulse W-band EPR spectrum of $Tyr_D^{\bullet}$ in Mn-depleted PsbA2-PSII. A similar spectrum was observed in all the samples studied here (data not shown). Spectra were measured using a two-pulse Hahn-echo sequence. A CW-like EPR spectrum is recovered from absorption spectrum by convolving the measured spectrum using a Bessel function of the 1st kind *i.e.* pseudo modulation. All three turning points (g_x, g_y and g_z) of the Tyr_Z radical spectrum are well resolved in addition to known proton hyperfine couplings [40,42,44–47]. This spectrum essentially represents the dark state spectrum. The corresponding $Tyr_Z^{\bullet}$ spectrum was obtained by illuminating the PSII sample approximately 5 s at 240 K in the presence of 5 mM ferricyanide. This spectrum contains a signal from both $Tyr_Z^{\bullet}$ and $Tyr_D^{\bullet}$. The $Tyr_Z^{\bullet}$ spectrum is obtained by subtracting the corresponding $Tyr_D^{\bullet}$ spectra recorded either before the illumination or upon annealing of the samples (both procedures resulted in similar $Tyr_Z^{\bullet}$ spectra). It is noted that the spectrum of $Tyr_Z^{\bullet}$ and $Tyr_D^{\bullet}$ are easily distinguished. The g_x component of $Tyr_Z^{\bullet}$ is significantly broader than the $Tyr_D^{\bullet}$ which is generally interpreted as a distribution in strength of the hydrogen-bonding due to some disorder in the protein environment around $Tyr_Z^{\bullet}$ [47], specifically about the phenolic oxygen. In addition the precise position of g_x decreases (in terms of g-value) suggesting phenolic oxygen occupies a less positive electrostatic environment.

Panel B in Fig. 5 shows $Tyr_Z^{\bullet}$ spectrum in the four PSII samples. In an earlier high field (235 GHz) EPR study, it was noted that the g_x position is shifted to lower g-value in PsbA2-PSII than in PsbA3-PSII [28], smaller but similar to the difference between $Tyr_Z^{\bullet}$ and $Tyr_D^{\bullet}$ suggesting the electrostatic environment of the phenolic oxygen is less positive

in PsbA2 *versus* PsbA3. The same small *g*-shift is observed for the W-band (94 GHz) data presented here. Interestingly it is also observed that the proton hyperfine couplings for the g_x turning point are resolved at this lower microwave frequency (94 *versus* 235 GHz), presumably because of a reduction in *g*-strain (heterogeneity of the B_0 field). This hyperfine structure is better resolved in PsbA2-PSII as compared to PsbA3-PSII suggesting a smaller distribution of microstates in PsbA2-PSII *versus* PsbA3-PSII. In other words, Tyr_Z adopts a more rigid conformation in PsbA2-PSII.

The high field EPR results described above compare well with earlier X-band (9 GHz) time-resolved measurements in intact PSII [28]. At this lower frequency the three unique g-values turning points of the Tyr_Z spectrum are unresolved but the hyperfine structure is readily observed. The X-band $Tyr_Z^{\bullet}$ spectrum $(S_3Tyr_Z^{\bullet})'$ in PsbA2-PSII as compared to PsbA3-PSII also displays a better resolves the hyperfine structure, reminiscent of that observed in the $Tyr_D^{\bullet}$ measured in the D2-His189Leu mutant, which disrupts the H-bond in which $Tyr_D^{\bullet}$ is involved [42]. Thus, both hyperfine and *g*-matrix data point to a weaker H-bond interaction between $Tyr_Z^{\bullet}$ and D1/His190 in PsbA2 *versus* PsbA3. As observed above, the high field EPR spectrum of PsbA3/Pro173Met-PSII is similar to PsbA2-PSII and the high field EPR spectrum of PsbA2/Met173Pro-PSII is similar to PsbA3-PSII further supporting the hypothesis that the Pro173 to Met substitution in PsbA3-PSII is mainly responsible for the observed changes in the g_x of $Tyr_Z^{\bullet}$ in PsbA2-PSII.

3.5. Time resolved absorption spectroscopy – Pro173Met exchange modifies the rereduction rate of $P_{680}^{+\bullet}$ by Tyr_Z

We then asked the question as to whether the Pro173 to Met substitution also determines the kinetics specificity of the oxidation of Tyr_Z in PsbA2-PSII and PsbA3-PSII. Fig. 6 shows the transient flash-induced absorption changes at 432 nm after the first (Panel A), second (Panel B), third (Panel C) and fourth flash (panel D) given to dark-adapted PsbA3-PSII (black symbols), PsbA2-PSII (red symbols), PsbA3/Pro173Met-PSII (blue symbols) and PsbA2/Met173Pro-PSII (green symbols). In this spectral region, the redox changes of several species, such as the chlorophylls, cytochromes, Tyr_Z, and Q_A, may contribute to the absorption profile. However, the most prominent spectral difference upon flash illumination is that associated with the bleaching of P_{680} upon its oxidation, which, in the blue region of the spectrum, peaks at 432 nm. In Fig. 5, the kinetics appeared indeed free of components originating from short lived excited state like uncoupled Chl*, for example, which would only contribute in the initial time point, decaying in a few ns. Panel A shows, as observed earlier [28], that after the first flash, *i.e.* in the S_1 state, the decay of $P_{680}^{+\bullet}$ was similar for both PsbA3-PSII and PsbA2-PSII throughout the studied time windows that cover the tens of ns to tens of μs range. As expected the Met173 to Pro mutation in PsbA2-PSII and the Pro173 to Met mutation in PsbA3-PSII did not result in significant alteration of the reduction of $P_{680}^{+\bullet}$ by Tyr_Z in the S_1 state. In contrast, in agreement with our

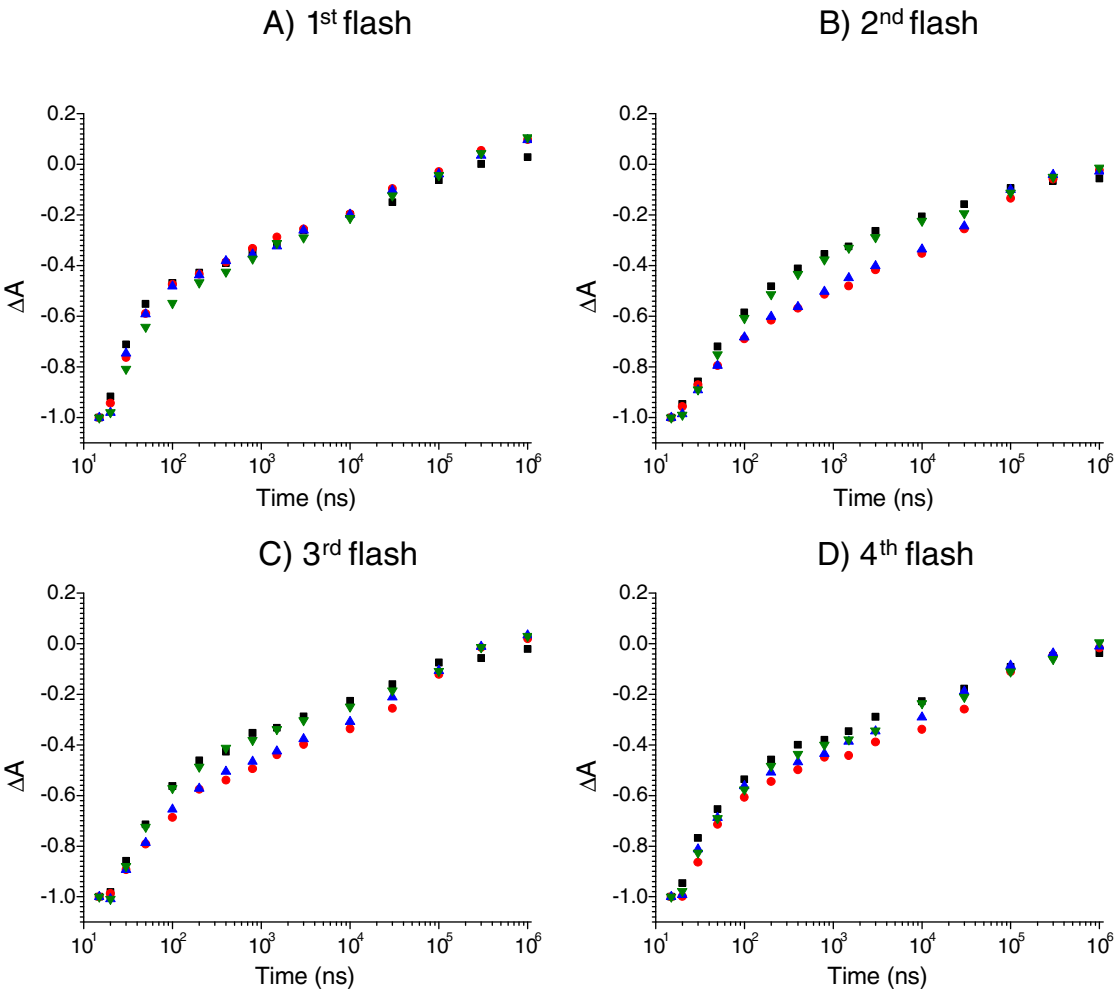

Fig. 6. Kinetics of flash-induced absorption changes measured at 432 nm in PsbA3-PSII (black symbols), in PsbA2-PSII (red symbols), in PsbA3/Pro173Met-PSII (blue symbols) and in PsbA2/Met173Pro-PSII (green symbols) after the 1st flash (Panel A), 2nd flash (Panel B), 3rd flash (Panel C and 4th flash (Panel D) given on dark-adapted PSII. [Chl] = 25 μg mL^{-1}. All the traces were normalized to −1. The original ΔI/I were all between -1.0×10^{10} and -1.2×10^{10}.

previous observations, after the second (Panel B) and third flash (Panel C), the components developing in the tens of μs in the decay of $P_{680}^{+\bullet}$ were markedly slowed in PsbA2-PSII with respect to PsbA3-PSII. The $P_{680}^{+\bullet}$ decay after the second flash in PsbA3-PSII and PsbA2-PSII has been fitted with multiple exponentials. Three components and a constant were sufficient to satisfyingly fit the data (see supplementary data). The fit yielded the following parameters for the fastest, intermediate and slowest components, respectively: $t_{1/2} \approx 34$ ns (57%) in PsbA3-PSII and $t_{1/2} \approx 32$ ns (44%) in PsbA2-PSII, $t_{1/2} \approx 0.79$ μs (22%) in PsbA3-PSII and $t_{1/2} \approx 1.01$ μs (21%) in PsbA2-PSII for the middle phase and $t_{1/2} \approx 33$ μs (16%) in PsbA3-PSII and $t_{1/2} \approx 49$ μs (31%) in PsbA2-PSII. This suggests that the most pronounced effect is a decrease in the amplitude of the fast phase in PsbA2-PSII versus PsbA3-PSII and a complementary increase in that of the slowest component, the intermediate components in the hundreds of ns undergoing only minor changes. According to the current understanding of the multiphasicity of the reduction of $P_{680}^{+\bullet}$, the sub-μs components are kinetically limited by the electron transfer process. In other words the rate reflects electron transfer from Tyr_Z to $P_{680}^{+\bullet}$ (but see [30]) and its amplitude is determined by the, low, equilibrium constant between $P_{680}^{+\bullet}Tyr_Z$ and $P_{680}Tyr_Z^{\bullet}$. The μs components reflect the progressive increase of this equilibrium constant resulting from, slower, proton release e.g. [48–50]. Recently Dau and coworkers further refined this framework by assigning more specifically the components developing in the hundreds of ns to structural rearrangement of the water network around the OEC, ensuing the formation of $[Tyr_Z^{\bullet}\text{-HN-His}]^+$ [51,52]. The present comparison of PsbA2-PSII and PsbA3-PSII, according to which the amplitude of the fastest and slowest components are affected in a complimentary manner is consistent with the equilibrium constant between $P_{680}^{+\bullet}Tyr_Z$ and $P_{680}Tyr_Z^{\bullet}$ being smaller in PsbA2-PSII than in PsbA3-PSII. In this framework, the slowed down μs components in PsbA2-PSII would reflect a hindered overall proton transfer upon oxidation of Tyr_Z by $P_{680}^{+\bullet}$. Notably, this hindrance would be particularly pronounced in the higher S states. After 4 flashes (Panel D), *i.e.* once the Mn_4CaO_5 cluster is mainly in the S_0 state, the progressive mixing of the S-states combined with the moderate amplitude of the period four oscillations in the $P_{680}^{+\bullet}$ decay kinetics make the data more equivocal. Nevertheless, the differences between the 4 samples were smaller than after the 2nd and 3rd flashes. Because the Cys144 and Pro173 in PsbA1 and PsbA3 which are exchanged for Pro and Met, respectively, in PsbA2 are in the loops that connect the α helices that respectively bear D1/His190 and Tyr_Z, we have previously proposed [28] that both the Cys144Pro and Pro173Met exchanges could affect the hydrogen bond between Tyr_Z and His-190 and/or the H-bond network in which these two side-chains are involved. The data in Fig. 6 bring support to this proposal as they show that the PsbA3/Pro173Met-PSII and PsbA2-PSII displayed similar kinetic characteristics and that, conversely PsbA2/Met173Pro-PSII resembled PsbA3-PSII. This identifies Pro173Met substitution in PsbA2-PSII as the main structural determinant of the observed changes in the $P_{680}^{+\bullet}$ decay.

4. Discussion

Because its φ backbone dihedral angle is locked, Pro is a singularly rigid amino acid. Its substitution for and by other residues in the vicinities of Tyr_Z and D1-His190 is thus expected to affect the overall orientation of the backbone skeleton downstream, *e.g.* [31], and to lead to significant structural consequences on the local environment of Tyr_Z, its H-bond network and the position of the water molecules near the water oxidizing site, *e.g.* [53–55] for recent reviews. We have therefore suggested in a previous study reporting functional differences between PsbA2-PSII and PsbA3-PSII that *i*) the Pro173Met exchange in PsbA2-PSII when compared to PsbA3-PSII was responsible for the observed changes and that *ii*) to keep a functional PSII, the Pro173Met exchange in PsbA2-PSII was compensated for by the additional 26 substitutions and, particularly, by the Cys144Pro exchange. Indeed, this amino acid is located in the α-helix C on the periplasmic side just before the α-helix bearing Tyr_Z (Fig. 1). To test the specific role of the Pro173 in PsbA3-PSII two site directed single mutants have been designed and studied; the Pro173Met-PsbA3-PSII and the Met173Pro-PsbA2-PSII.

Due to the structural singularity of Pro mentioned just above and to its position in the PsbA sequence, it could be concluded that targeting this residue by site directed mutagenesis may result in large structural changes resulting in a destabilized PSII complex or in the disassembly of the catalytic cluster. That this was not the case can be concluded from the observation that mutant cells grew similarly to their respective control strains. We then showed that the single substitution Pro173Met in PsbA3-PSII and Met173Pro in PsbA2-PSII resulted in O_2 evolving PSII with rates commensurate to those obtained with the control PSII. Then, we compared the mutants and controls with respect to the functional phenotypes described previously, which differentiate PsbA2-PSII and PsbA3-PSII from each other. Remarkably, in PsbA2-PSII and PsbA3-PSII, the differences found were specific to the $Tyr_Z^{\bullet}$, both in terms of its EPR spectroscopic features and of its oxidation rate in the presence of the S_2 and S_3 states. Indeed, we checked that the EPR multiline signal associated with the formation of S_2, which is notoriously sensitive to structure changes [56], and found that it was indistinguishable in the two types of PSII. Similarly, the rate of the $(S_3Tyr_Z^{\bullet})'$ to S_0Tyr_Z transition was similar in PsbA2-PSII and PsbA3-PSII [28]. From these observations we thus concluded that the structure of theMn_4CaO_5 cluster remains unchanged upon the PsbA exchange. In contrast; *i*) the μs components of kinetics of reduction of $P_{680}^{+\bullet}$ by Tyr_Z in the S_2 and S_3 states was found significantly slowed down and *ii*) the split EPR signal induced by near infrared illumination at ≈4 K in the S_3 state was strongly affected both in term of yield and spectral shape. In both cases, we show here that the single mutation Met173Pro in the PsbA2 gene nicely mimicks the PsbA3-PSII specificity and *vice versa*. This shows that the Pro173Met mutation is the main structural determinant of these functional differences.

The study of the kinetics of reduction of $P_{680}^{+\bullet}$ by Tyr_Z as a function of the flash number (*i.e.* the S_i states) in the four different PSII samples reveals another interesting feature: Whereas the kinetics, more specifically the components developing in the tens of μs, were markedly slower in the S_2 and S_3 states, in the PsbA2-PSII and PsbA3Pro173Met-PSII with respect to their respective controls, they were hardly dependent on whether the residue at position 173 is a Pro or a Met in the S_1 states (in S_0 the results are more ambiguous owing to the unavoidable scrambling of the S-states after 4 flashes). This shows that these mutations do not significantly increase, at least in the S_1 state, the yield of the $P_{680}^{+\bullet}Q_A^{-\bullet}$ charge recombination, which occurs in the hundreds of μs time range, *e.g.* [49]. This conclusion also most likely applies to the following S_n states since the use of PPBQ prevents the formation of stable $Q_B^{-\bullet}$ so that the acceptor side is in the same redox state after each flash in the series. Thus, it is very unlikely that the slower $P_{680}^{+\bullet}$ reduction detected on the second and following flashes originates from a different yield of $P_{680}^{+\bullet}Q_A^{-\bullet}$ charge recombination. In addition, although the reduction of $P_{680}^{+\bullet}$ by Tyr_Z in the S_3 state is much slower in PsbA2-PSII than in PsbA3-PSII, this slowing down could not be detectable in the kinetics measured at 292 nm in [28]. Indeed, the first time point was measured 15 μs after the third flash *i.e.* in a time range where, from the data in Fig. 6C, the differences between the two samples become less marked.

Also seen in the four samples studied here, is that the reduction of $P_{680}^{+\bullet}$ in the tens of ns time range is only slightly affected whatever the S_n state, including S_1, *i.e.* in a transition in which no proton is released. This result strongly indicates that: *i*) the possible slight modification of distance and angle between the Tyr_Z and the His190 upon the Pro173Met exchange hardly affects the pure electron transfer from Tyr_Z to $P_{680}^{+\bullet}$ and *ii*) in the light of the marked slow-down of the reduction of $P_{680}^{+\bullet}$ in S_2 and S_3, it is, under all likelihood, the H-bond network which is involved in the release of the proton, when it occurs, which is affected by the Pro173Met exchange. According to the current

understanding of the rates and amplitudes of the various kinetic components of the oxidation of Tyr_Z, those developing in the tens of μs are kinetically limited by the rate of the electrostatic relaxation associated with the transfer of H^+ triggered by the oxidation of Tyr_Z by $P_{680}^{+\bullet}$ [48,50]. This relaxation results in a progressive increase in the equilibrium constant of the $P_{680}^{+\bullet}Tyr_Z$ to $P_{680}Tyr_Z^{\bullet}$ reaction. Consequently, in this framework, the amplitudes of these slow components are directly related to this equilibrium constant and the fact that they vary with the S-states reflects the dependence upon the S-states of the driving force of the electron transfer reaction between $P_{680}^{+\bullet}$ and Tyr_Z. In line with this, the sub-stoichiometric H^+ release associated with the S_1 to S_2 transitions, *e.g.* [57,58], leaves a positive charge in the catalytic cluster not fully compensated and hence results, via Coulombic effects, in a decrease in the driving force of the electron transfer reaction between $P_{680}^{+\bullet}$ and Tyr_Z [59], for a review. In this framework, the sluggishness of the μs components in PsbA2-PSII with respect to PsbA3-PSII is readily interpreted by postulating that the H-bond network involved in this relaxation process differs and this assumption is supported by the differences in the width of the g_x component of the $Tyr_Z^{\bullet}$ tensor in the two cases. Yet, the fact that these differences only become apparent in the presence of S_2 and S_3 would imply that this H-bond network is reorganized upon the formation of S_2, or that, in other terms, the consequences of the formation of S_2 on the μs components of $P_{680}^{+\bullet}$ reduction is not merely Coulombic but also structural. In agreement with this model, it has been proposed that the geometry of the cluster of four water molecules involved in the Mn_4CaO_5-Tyr_Z motif is playing an important role in the stabilization of an unusual short distance between Tyr_Z and His190 [60]. In a theoretical work [61], it has been proposed that Tyr_Z oxidation leads to the reorientation of the dipole moment of the Mn_4CaO_5 cluster such that the locus of negative charge is directed towards W1, the H_2O bound to Mn4, and its hydrogen bonding partner D1-Asp61 resulting into the deprotonation of W1. Since the water molecules around Tyr_Z and mentioned above are part of the same proton network that includes the D1-Asp61, this cluster of water molecules can play a role in the proton release upon Tyr_Z oxidation as also proposed recently [62]. The present data show that substituting Pro173 for Met and *vice versa* mimics the respective the PsbA2 for PsbA3 substitution (and *vice versa*) so that this mutation has structural consequences on the H-bond network in which Tyr_Z is involved and, more specifically, on the way this network is reorganized upon the formation of S_2.

Acknowledgements

This study was supported by JST-PRESTO program (4018 for M.S.) and Grant-in-Aid for scientific research from the Ministry of Education, Science, Sports, Culture and Technology (21612007 for M.S.). AB was supported by the French Infrastructure for Integrated Structural Biology (FRISBI) ANR-10-INSB-05-01 and the CEA/DSV "Bioénergie" program. FR acknowledges financial support from the CNRS and the "Initiative d'Excellence" program from the French state (Grant "DYNAMO", ANR-11-LABX-0011-01).

Appendix A. Supplementary data

Supplementary data to this article can be found online at http://dx.doi.org/10.1016/j.bbabio.2014.08.008. Fits of the P680+ decay.

References

[1] Y. Umena, K. Kawakami, J-R. Shen, N. Kamiya, Crystal structure of oxygen-evolving Photosystem II at a resolution of 1.9 Å, Nature 473 (2011) 55–60.
[2] F.H.M. Koua, Y. Umena, K. Kawakami, J.-R. Shen, Structure of Sr-substituted Photosystem II at 2.1 angstrom resolution and its implications in the mechanism of water oxidation, Proc. Natl. Acad. Sci. U. S. A. 110 (2013) 3389–3894.
[3] B.A. Diner, F. Rappaport, Structure, dynamics, and energetic of the primary photochemistry of Photosystem II of oxygenic photosynthesis, Annu. Rev. Plant Biol. 53 (2002) 551–580.
[4] G. Renger, Light-induced oxidative water splitting in photosynthesis: energetics, kinetics, and mechanism, J. Photochem. Photobiol. B 104 (2011) 35–43.
[5] H. Dau, I. Zaharieva, M. Haumann, Recent developments in research on water oxidation by photosystem II, Curr. Opin. Chem. Biol. 16 (2012) 3–10.
[6] B. Kok, B. Forbush, M. McGloin, Cooperation of charges in photosynthetic O_2 evolution-I. A linear four step mechanism, Photochem. Photobiol. 11 (1970) 457–475.
[7] P. Joliot, B. Kok, Oxygen evolution in photosynthesis, in: Govindjee (Ed.), Bioenergetics of photosynthesis, Academic Press, New York, 1975, pp. 387–412.
[8] N. Cox, J. Messinger, Reflections on substrate water and dioxygen formation, Biochim. Biophys. Acta 1827 (2013) 1020–1030.
[9] J. Yano, V. Yachandra, Mn_4Ca cluster in photosynthesis: Where and how water is oxidized to dioxygen, Chem. Rev. 114 (2014) 4175–4205.
[10] A.K. Clarke, A. Soitamo, P. Gustafsson, G. Oquist, Rapid interchange between two distinct forms of cyanobacterial photosystem II reaction-center protein D1 in response to photoinhibition, Proc. Natl. Acad. Sci. U. S. A. 90 (1993) 9973–9977.
[11] S.S. Golden, Light-responsive gene expression in cyanobacteria, J. Bacteriol. 177 (1995) 1651–1654.
[12] J. Komenda, H. Hassan, B.A. Diner, R.J. Debus, J. Barber, P.J. Nixon, Degradation of the Photosystem II D1 and D2 proteins in different strains of the cyanobacterium *Synechocystis* PCC 6803 varying with respect to the type and level of *psbA* transcript, Plant Mol. Biol. 42 (2000) 635–645.
[13] C.I. Sicora, S.E. Appleton, C.M. Brown, J. Chung, J. Chandler, A.M. Cockshutt, I. Vass, D.A. Campbell, Cyanobacterial *psbA* families in *Anabaena* and *Synechocystis* encode trace, constitutive, and UVB-induced D1 isoforms, Biochim. Biophys. Acta 1757 (2006) 47–56.
[14] P.B. Kós, Z. Deák, O. Cheregi, I. Vass, Differential regulation of *psbA* and *psbD* gene expression, and the role of the different D1 protein copies in the cyanobacterium *Thermosynechococcus elongatus* BP-1, Biochim. Biophys. Acta 1777 (2008) 74–83.
[15] P. Mulo, C. Sicora, E.-M. Aro, Cyanobacterial *psbA* gene family: optimization of oxygenic photosynthesis, Cell. Mol. Life Sci. 66 (2009) 3697–3710.
[16] C.I. Sicora, F.M. Ho, T. Salminen, S. Styring, E.-M. Aro, Transcription of a "silent" cyanobacterial *psbA* gene is induced by microaerobic conditions, Biochim. Biophys. Acta 1787 (2009) 105–112.
[17] M. Sugiura, Y. Kato, R. Takahashi, H. Suzuki, T. Watanabe, T. Noguchi, F. Rappaport, A. Boussac, Energetics in Photosystem II from *Thermosynechococcus elongatus* with a D1 protein encoded by either the $psbA_1$ or $psbA_3$ gene, Biochim. Biophys. Acta 1797 (2010) 1491–1499.
[18] E. Kiss, P.B. Kos, M. Chen, I. Vass, A unique regulation of the expression of the *psbA*, *psbD*, and *psbE* genes, encoding the D1, D2 and cytochrome b_{559} subunits of the Photosystem II complex in the chlorophyll d containing cyanobacterium *Acaryochloris marina*, Biochim. Biophys. Acta 1817 (2012) 1083–1094.
[19] T.C. Summerfield, J. Toepel, L.A. Sherman, Low-oxygen induction of normally cryptic *psbA* genes in cyanobacteria, Biochemistry 47 (2008) 12939–12941.
[20] X. Zhang, L.A. Sherman, Alternate copies of D1 are used by cyanobacteria under different environmental conditions, Photosynth. Res. 114 (2012) 133–135.
[21] J.W. Murray, Sequence variation at the oxygen-evolving centre of photosystem II: a new class of 'rogue' cyanobacterial D1 proteins, Photosynth. Res. 110 (2012) 177–184.
[22] P. Mulo, I. Sakurai, E.-M. Aro, Strategies for psbA gene expression in cyanobacteria, green algae and higher plants: From transcription to PSII repair, Biochim. Biophys. Acta 1817 (2012) 247–257.
[23] M. Sugiura, C. Azami, K. Koyama, A.W. Rutherford, F. Rappaport, A. Boussac, Modification of the pheophytin redox potential in *Thermosynechococcus elongatus* Photosystem II with PsbA3 as D1, Biochim. Biophys. Acta 1837 (2013) 139–148.
[24] Y. Nakamura, T. Kaneko, S. Sato, M. Ikeuchi, H. Katoh, S. Sasamoto, A. Watanabe, M. Iriguchi, K. Kawashima, T. Kimura, Y. Kishida, C. Kiyokawa, M. Kohara, M. Matsumoto, A. Matsuno, N. Nakazaki, S. Shimpo, M. Sugimoto, C. Takeuchi, M. Yamada, S. Tabata, Complete genome structure of the thermophilic cyanobacterium *Thermosynechococcus elongatus* BP-1, DNA Res. 9 (2002) 123–130.
[25] B. Loll, M. Broser, P.B. Kós, J. Kern, J. Biesiadka, I. Vass, W. Saenger, A. Zouni, Modeling of variant copies of subunit D1 in the structure of Photosystem II from *Thermosynechococcus elongatus*, Biol. Chem. 389 (2008) 609–617.
[26] J. Sander, M. Nowaczyk, J. Buchta, H. Dau, I. Vass, Z. Deak, M. Dorogi, M. Iwai, M. Rogner, Functional characterization and quantification of the alternative PsbA copies in *Thermosynechococcus elongatus* and their role in photoprotection, J. Biol. Chem. 285 (2010) 29851–29856.
[27] M. Sugiura, A. Boussac, Some Photosystem II properties depending on the D1 protein variants in *Thermosynechococcus elongatus*, Biochim. Biophys. Acta 1837 (2014) 1427–1434.
[28] M. Sugiura, S. Ogami, M. Kusumi, S. Un, F. Rappaport, A. Boussac, Environment of Tyr_Z in Photosystem II from *Thermosynechococcus elongatus* in which PsbA2 is the D1 protein, J. Biol. Chem. 287 (2012) 13336–13347.
[29] A.M.A. Hays, I.R. Vassiliev, J.H. Golbeck, R.J. Debus, Role of D1-His190 in the proton-coupled oxidation of tyrosine Y_Z in manganese-depleted Photosystem II, Biochemistry 38 (1999) 11851–11865.
[30] F. Rappaport, A. Boussac, D.A. Force, J. Peloquin, M. Brynda, M. Sugiura, S. Un, R.D. Britt, B.A. Diner, Probing the coupling between proton and electron transfer in Photosystem II core complexes containing a 3-fluorotyrosine, J. Am. Chem. Soc. 131 (2009) 4425–4433.
[31] F.S. Cordes, J.N. Bright, M.S.P. Sansom, Proline-induced distorsions of transmembrane helices, J. Mol. Biol. 323 (2002) 951–960.
[32] M. Sugiura, A. Boussac, T. Noguchi, F. Rappaport, Influence of Histidine-198 of the D1 subunit on the properties of the primary electron donor, P680, of Photosystem II in *Thermosynechococcus elongatus*, Biochim. Biophys. Acta 1777 (2008) 331–342.

[33] M. Sugiura, Y. Inoue, Highly purified thermo-stable oxygen evolving Photosystem II core complex from the thermophilic cyanobacterium *Synechococcus elongatus* having His-tagged CP43, Plant Cell Physiol. 40 (1999) 1219–1231.
[34] D. Beal, F. Rappaport, P. Joliot, A new high-sensitivity 10-ns time-resolution spectrophotometric technique adapted to in vivo analysis of the photosynthetic apparatus, Rev. Sci. Instrum. 70 (1999) 202–207.
[35] S. Styring, A.W. Rutherford, In the oxygen-evolving complex of Photosystem II the S_0-state is oxidized to the S_1-state by D^+ (Signal-II slow), Biochemistry 26 (1987) 2401–2405.
[36] A. Boussac, K. Koyama, M. Sugiura, The Tll0287 protein is a hemoprotein associated with the PsbA2-Photosystem II complex in *Thermosynechococcus elongatus*, Biochim. Biophys. Acta 1827 (2013) 1174–1182.
[37] V. Petrouleas, D. Koulougliotis, N. Ioannidis, Trapping of metalloradical intermediates of the S-states at liquid helium temperatures. Overview of the phenomenology and mechanistic implications, Biochemistry 44 (2005) 6723–6728.
[38] A. Boussac, M. Sugiura, T.-L. Lai, A.W. Rutherford, Low temperature photochemistry in Photosystem II from *Thermosynechococcus elongatus* induced by visible and near-infrared light, Philos. Trans. R. Soc. 363 (2008) 1203–1210.
[39] Y. Sanakis, N. Ioannidis, G. Sioros, V. Petrouleas, A novel S = 7/2 configuration of the Mn cluster of photosystem II, J. Am. Chem. Soc. 123 (2001) 10766–10767.
[40] H. Mino, A. Kawamori, Microenvironments of tyrosine D^+ and tyrosine Z^+ in Photosystem II studied by proton matrix ENDOR, Biochim. Biophys. Acta 1185 (1994) 213–220.
[41] A. Boussac, N. Ishida, M. Sugiura, F. Rappaport, Probing the role of chloride in Photosystem II from *Thermosynechococcus elongatus* by exchanging chloride for iodide, Biochim. Biophys. Acta 1817 (2012) 802–810.
[42] S. Un, A. Boussac, M. Sugiura, Characterization of the tyrosine-Z radical and its environment in the spin-coupled $S_2Tyr_Z^{\bullet}$ state of Photosystem II from *Thermosynechococcus elongatus*, Biochemistry 46 (2007) 3138–3150.
[43] P. Dorlet, A. Boussac, A.W. Rutherford, S. Un, Multifrequency high-field EPR study of the interaction between the tyrosyl Z radical and the manganese cluster in plant photosystem II, J. Phys. Chem. B 103 (1999) 10945–10954.
[44] C. Tommos, X.S. Tang, K. Warncke, C.W. Hoganson, S. Styring, J. Mc-Cracken, B.A. Diner, G.T. Babcock, Spin-density distribution, conformation, and hydrogen-bonding of the redox-active tyrosine Y-Z in Photosystem II from multiple electron magnetic-resonance spectroscopies: implications for photosynthetic oxygen evolution, J. Am. Chem. Soc. 117 (1995) 10325–10335.
[45] S. Un, L.C. Brunel, T.M. Brill, J.-L. Zimmermann, A.W. Rutherford, Angular orientation of the stable tyrosyl radical within Photosystem II by high-field 245-GHz electron paramagnetic resonance, Proc. Natl. Acad. Sci. U. S. A. 91 (1994) 5262–5266.
[46] C. Teutloff, S. Pudollek, S. Kessen, M. Broser, A. Zouni, R. Bittl, Electronic structure of the tyrosine D radical and the water-splitting complex from pulsed ENDOR spectroscopy on photosystem II single crystals, Phys. Chem. Chem. Phys. 11 (2009) 6716–6726.
[47] S. Un, X.S. Tang, B.A. Diner, 245 GHz high-field EPR study of tyrosine-D degrees and tyrosine-Z degrees in mutants of photosystem II, Biochemistry 35 (1996) 679–684.
[48] M.J. Schilstra, F. Rappaport, J.H. Nugent, C.J. Barnett, D.R. Klug, Proton/hydrogen transfer affects the S state-dependent microsecond phases of P_{680}^+ reduction during water splitting, Biochemistry 37 (1998) 3974–3981.
[49] P. Kuhn, H. Eckert, H.J. Eichler, G. Renger, Analysis of the P_{680}^+ reduction pattern and its temperature dependence in oxygen evolving PSII core complexes from a thermophilic cyanobacteria and higher plants, Phys. Chem. Chem. Phys. 6 (2004) 4838–4843.
[50] G. Christen, G. Renger, The role of hydrogen bonds for the multiphasic P_{680}^+ reduction by Y_Z in photosystem II with intact oxygen evolution capacity: analysis of kinetic H/D isotope exchange effects, Biochemistry 38 (1999) 2068–2077.
[51] R.J. Debus, FTIR studies of metal ligands, networks of hydrogen bonds, and water molecules near the active site Mn_4CaO_5 cluster in photosystem II, Biochim. Biophys. Acta (2014), http://dx.doi.org/10.1016/j.bbabio.2014.07.007 (in press).
[52] T. Noguchi, Fourier transform infrared difference and time-resolved infrared detection of the electron and proton transfer dynamics in photosynthetic water oxidation, Biochim. Biophys. Acta (2014), http://dx.doi.org/10.1016/j.bbabio.2014.06.009 (in press).
[53] H. Bao, P.L. Dilbeck, R. Burnap, Proton transport facilitating water-oxidation: the role of second sphere ligands surrounding the catalytic metal cluster, Photosynth. Res. 116 (2013) 215–229.
[54] A. Klauss, M. Haumann, H. Dau, Alternating electron and proton transfer steps in photosynthetic water oxidation, Proc. Natl. Acad. Sci. U. S. A. 109 (2012) 16035–16040.
[55] A. Klauss, T. Sikora, B. Suss, H. Dau, Fast structural changes (200–900 ns) may prepare the photosynthetic manganese complex for oxidation by the adjacent tyrosine radical, Biochim. Biophys. Acta 1817 (2012) 1196–1207.
[56] N. Cox, D.A. Pantazis, F. Neese, W. Lubitz, Biological water oxidation, Acc. Chem. Res. 46 (2013) 1588–1596.
[57] F. Rappaport, J. Lavergne, Proton release during successive oxidation steps of the photosynthetic water oxidation process: stoichiometries and pH dependence, Biochemistry 30 (1991) 10004–10012.
[58] H. Suzuki, M. Sugiura, T. Noguchi, Monitoring proton release during photosynthetic water oxidation in Photosystem II by means of isotope-edited infrared spectroscopy, J. Am. Chem. Soc. 131 (2009) 7849–7857.
[59] F. Rappaport, B.A. Diner, Primary photochemistry and energetics leading to the oxidation of the $(Mn)_4Ca$ cluster and to the evolution of molecular oxygen in Photosystem II, Coord. Chem. Rev. 252 (2008) 259–272.
[60] K. Saito, J.R. Shen, T. Ishida, H. Ishikita, Short hydrogen bond between redox-active tyrosine Y_Z and D1-His-190 in the photosystem II crystal structure, Biochemistry 50 (2011) 9836–9844.
[61] M. Retegan, N. Cox, W. Lubitz, D.A. Pantazis, The first tyrosyl radical intermediate formed in the S_2-S_3 transition of Photosystem II, Phys. Chem. Chem. Phys. 16 (2014) 11901–11910.
[62] S. Nakamura, R. Nagao, R. Takahashi, T. Noguchi, Fourier transform infrared detection of a polarizable proton trapped between photooxidized Tyrosine Y_Z and a coupled Histidine in Photosystem II: Relevance to the proton transfer mechanism of water oxidation, Biochemistry 53 (2014) 3131–3144.